



THE UNIVERSITY *of* EDINBURGH

Edinburgh Research Explorer

## Solid-state Li-ion batteries with carbon microfiber electrodes via 3D electrospinning

**Citation for published version:**

Arrese-Igor, M, Vong, M, Orue, A, Kassanos, P, George, C, Aguesse, F, Mysyk, R, Radacsi, N & López-Aranguren, P 2023, 'Solid-state Li-ion batteries with carbon microfiber electrodes via 3D electrospinning', *Applied Physics Letters*, vol. 122, no. 17, 173903. <https://doi.org/10.1063/5.0151949>

**Digital Object Identifier (DOI):**

[10.1063/5.0151949](https://doi.org/10.1063/5.0151949)

**Link:**

[Link to publication record in Edinburgh Research Explorer](#)

**Document Version:**

Peer reviewed version

**Published In:**

Applied Physics Letters

**General rights**

Copyright for the publications made accessible via the Edinburgh Research Explorer is retained by the author(s) and / or other copyright owners and it is a condition of accessing these publications that users recognise and abide by the legal requirements associated with these rights.

**Take down policy**

The University of Edinburgh has made every reasonable effort to ensure that Edinburgh Research Explorer content complies with UK legislation. If you believe that the public display of this file breaches copyright please contact [openaccess@ed.ac.uk](mailto:openaccess@ed.ac.uk) providing details, and we will remove access to the work immediately and investigate your claim.



This is the author's peer reviewed, accepted manuscript. However, the online version of record will be different from this version once it has been copyedited and typeset.

PLEASE CITE THIS ARTICLE AS DOI: 10.1063/1.50151949

## Solid-state Li-ion batteries with Carbon Micro Fibre Electrodes via 3D Electrospinning

Mikel Arrese-Igor<sup>1,2</sup>, Michel Vong<sup>3</sup>, Ander Orue<sup>1</sup>, Panagiotis Kassanos<sup>4</sup>, Chandramohan George<sup>5</sup>, Frédéric Aguesse<sup>1</sup>, Roman Mysyk<sup>1</sup>, Norbert Radacsi<sup>3</sup>, Pedro López-Aranguren<sup>\*1</sup>

<sup>1</sup> Centre for Cooperative Research on Alternative Energies (CIC energiGUNE), Basque Research and Technology Alliance (BRTA), Alava Technology Park, Albert Einstein 48, 01510 Vitoria-Gasteiz, Spain

<sup>2</sup> University of the Basque Country (UPV/EHU), Barrio Sarriena, s/n, 48940 Leioa, Spain.

<sup>3</sup> School of Engineering, Institute for Materials and Processes, The University of Edinburgh, King's Buildings, Edinburgh, United Kingdom

<sup>4</sup>The Hamlyn Centre, Imperial College London, SW7 2AZ London, United Kingdom

<sup>5</sup> Dyson School of Design Engineering, Imperial College London, London SW7 1NA, UK

\*Corresponding author: [plopez@cicenergigune.com](mailto:plopez@cicenergigune.com)

Keywords:

3D electrospinning, carbon fibers, Lithium-Ion Battery, Solid-State Battery, Poly(ethylene) oxide

### ABSTRACT

Self-standing carbon fiber electrodes hold promise for solid-state battery technology owing to their networked structures improving interparticle connectivity, robustness contributing to mechanical integrity, and surface sites confining Li dendrites. We here evaluate carbonized 3D electrospun fibers filled with polymer electrolytes as anodes in solid-state lithium half cells. Microscopic analysis of the cells demonstrates the high wettability of carbon fibers with electrolytes, promoting an intimate contact between electrolytes and fibers. Solid-state cells delivered high initial capacities up to ~300 mAh/g, although the latter cycles were characterized by gradual capacity fade (~100 mAh/g in the 100<sup>th</sup> cycle with nearly 100% coulombic efficiency), attributed to the onset of parasitic reactions increasing the cell resistance and polarization. When these were benchmarked against similar cells but with the liquid electrolyte, it was found that Li storage in these fiber electrodes is intermediate between graphite and hard carbon in terms of lithiation voltage (vs. Li/Li<sup>+</sup>), corroborating with the nature of carbon assessed by XRD and

This is the author's peer reviewed, accepted manuscript. However, the online version of record will be different from this version once it has been copyedited and typeset.

PLEASE CITE THIS ARTICLE AS DOI: 10.1063/1.50151949

Raman analysis. These observations can contribute to further development and optimization of solid-state batteries with 3D electrospun carbon fiber electrodes.

Despite the high volumetric and gravimetric energy density ( $\sim 700 \text{ Wh}\cdot\text{l}^{-1}$  and  $\sim 250 \text{ Wh}\cdot\text{kg}^{-1}$ ) of Li-ion batteries (LIBs) [1–3], the use of organic liquid electrolytes limits their maximum energy density, safety, and operating temperature, presenting roadblocks to their adoption in electric vehicles [4–7] and beyond. Replacing liquid electrolytes with solid electrolytes that are nonflammable can overcome this limitation [8] but requires suitable electrode architectures to facilitate a high concentration of point contacts between electrolytes and active particles for facile Li exchange. For example, solid polymer electrolytes (SPEs) based on poly(ethylene) oxide (PEO) can be processed into thin membranes of 30–50  $\mu\text{m}$  to yield conductivities of  $10^{-3}$ – $10^{-4} \text{ S cm}^{-1}$  at 70  $^{\circ}\text{C}$  while ensuring an intimate contact with electrode surfaces [6,9].

Solid-state batteries (SSBs) rely on the use of a Li metal anode, which has high theoretical capacity of  $\sim 3800 \text{ mAh}\cdot\text{g}^{-1}$  [10]. However, the cells with Li metal suffer from high interfacial resistance [11], lithium dendrites [12], or solid electrolyte-lithium metal parasitic reactions [13], leading to suboptimal battery performance, which impedes further progress and deployment of this technology [14–16]. Therefore, carbon-based electrodes that are typically used in traditional LIBs still represent a safe and low-cost alternative for SSBs [17]. These electrodes offer a reduction potential as close as Li metal (0.1 V vs.  $\text{Li}/\text{Li}^+$ ) [18], and despite their lower capacity, they are preferable when considering the trade-off among the safety, performance, and longevity of batteries [16,19]. Other active material alternatives for the negative electrode comprises the use of silicon; however, large volume expansion of around 400% during charge and rapid capacity fading do not allow for its direct implementation. Therefore, it is of particular interest the combination of carbon-based negative electrodes with silicon to progress toward high-energy density and long-lasting batteries [20]. Among available carbon materials, one-dimensional structures such as carbon nanofibers are the most desirable ones due to their short lengths for ionic transport, and efficient one-dimensional electron transport along the longitudinal direction [21]. These materials show a potentially increased capacity as active material compared to conventional

This is the author's peer reviewed, accepted manuscript. However, the online version of record will be different from this version once it has been copyedited and typeset.

PLEASE CITE THIS ARTICLE AS DOI: 10.1063/1.50151949

intercalation mechanism ( $\text{LiC}_6$ ) in graphite as they are often able to store lithium on both sides of the graphene layers [22,23], and their electrochemical performance is similar to or better than that of graphite in liquid electrolyte [23,24]. Among several techniques, electrospinning has been highlighted as a scalable, relatively simple, rapid, and low-cost method for carbon fiber fabrication, which allows for fiber sized down to 20 nm, with a high surface area and thin web morphology, potentially increasing Li storage capacity [24–26]. Electrospun carbon nanofibers as anodes have been shown to outperform other carbonaceous materials in terms of Li storage capacity [18,21,24]. In the last few years, an advanced electrospinning technique was developed by combining 3D printing and electrospinning [27]. This technology allows the fabrication of designed 3D macrostructures with micro- to nano-fibrous features. The 3D structures are fabricated in a single step in a 10-minute electrospinning experiment, and the structures could reach a height of about 3–4 cm [27]. Recently, this technology has been applied to fabricate 3D structures made of Polyacrylonitrile (PAN), a commonly used precursor for carbon nanofibers [28].

However, in designing SSB electrodes, several factors must be considered before applying carbon fibers as anodes: *i*) a robust ionic conductivity network must be ensured by the wetting of the active material with the solid electrolyte. *ii*) maintaining an intimate interface between carbon fiber and solid electrolytes (seamless integration over cycling). *iii*) chemical stability of the interfaces created over cycling, and *iv*) overall mechanical integrity of the sandwich structures. *v*) minimizing the side reactions contributing to premature cell failure. These issues are still poorly understood, especially for the free-standing 3D carbon fibers as anodes in the context of solid-state batteries. In addition, the brittleness of carbon nanofiber structures hampers their processing into solid-state electrodes [29]. In this work, we demonstrate the use of carbon microfiber electrodes obtained via 3D electrospinning and posterior carbonization (3DeCMFs). The electrochemical properties of these carbon fibers in both solid-state cells (with a PEO SPE) and liquid electrolyte cells were compared using Li half-cells. The liquid cells delivered a reversible capacity of  $300 \text{ mAh}\cdot\text{g}^{-1}$  with nearly 100% CE, while solid-state cells delivered a capacity ~of

This is the author's peer reviewed, accepted manuscript. However, the online version of record will be different from this version once it has been copyedited and typeset.

PLEASE CITE THIS ARTICLE AS DOI: 10.1063/1.50151949

150 mAh·g<sup>-1</sup> with 100% CE, and the capacity was found to be gradually fading due to increased cell resistance and polarization over cycling. Li storage in these is found to be intermediate between graphite and hard carbon, and takes place at more negative potentials compared to liquid electrolyte cells.

Figure 1 schematizes the preparation of half-cells with Li metal and the 3DeCMF mat electrode in liquid electrolyte, using a glass fiber (GF) separator impregnated with 200  $\mu$ L of the liquid electrolyte. The electrodes for solid-state cells were prepared by adding the PEO:LiBOB-ACN mixture onto the porous carbon fibers. The composite electrode was dried overnight at 50 °C under a vacuum to remove the solvent prior to cell assembly. For the solid-state cells, an SPE membrane with a 16 mm diameter was used as the separator and the electrolyte.

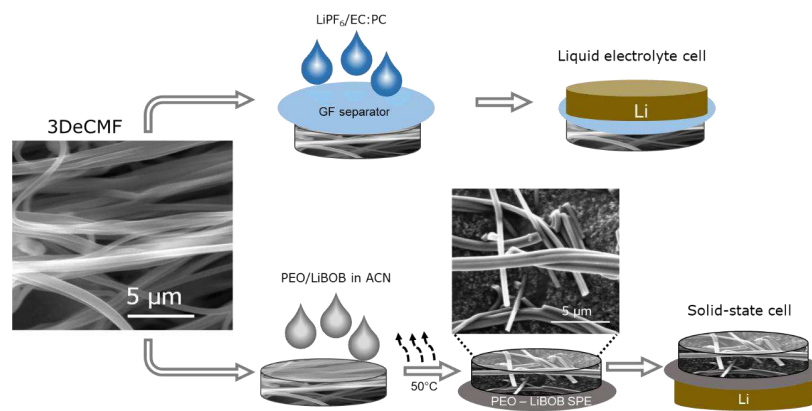


FIG1. Schematic representation of the liquid and solid-state cell electrode processing and cell configuration.

Unlike the typical electrospinning of polyacrylonitrile (PAN) onto substrates and peeling off, 3D electrospinning allows obtaining electrospun webs since the liquid PAN solution can be simply turned into a solid white fibrous material (Figure 2a and Figure S1), which can be carbonized to achieve 3DeCMFs (Figure 2b). There were no significant morphological changes observed, except for a small volume reduction that was expected as the polymer decomposes upon heating.

This is the author's peer reviewed, accepted manuscript. However, the online version of record will be different from this version once it has been copyedited and typeset.

PLEASE CITE THIS ARTICLE AS DOI: 10.1063/1.50151949

The obtained meshes are soft and flexible 3D sponge-like structures formed by smooth fibers. The transformation of the PAN nanofiber into carbon-fiber structure was carried out through a two-step process: stabilization and carbonization. The stabilization of electrospun fibers (250 °C for 2 h under N<sub>2</sub>) is performed to cross-link PAN chains and prepare a structure able to withstand a high-temperature carbonization treatment [30]. The carbonization step (850 °C for 1h under N<sub>2</sub>; 5 °C·min<sup>-1</sup>) turned the electrospun fibers into black-colored 3DeCMFs. Consequently, 3DeCMFs present homogeneous 1D structures (SEM, Figure 2c) without fiber ruptures and significant deformation/stretching after carbonization. The fiber diameter is maintained between 300 and 800 nm. Sheet resistance measurements were carried out on these samples. The carbonized 3DeCMFs (Figure 2b) showed a sheet resistance of ~393.21 Ω/square, and the pressed electrodes displayed a sheet resistance of ~245.92 Ω/square (Figure S2). In addition, mechanical tests of these have been carried out, and the stress-strain curves of these samples are shown in Figure S3. In brief, the mechanical properties of the 3DeCMFs showed reasonable Young's moduli up to 160 Pa, although the pressed samples showed a decreased value of ~10.6 Pa.

Nitrogen and CO<sub>2</sub> adsorption analyses were performed to evaluate the surface area, micropore volume, total pore volume, and pore size distribution of 3DeCMFs. The nitrogen adsorption isotherm in Figure 2d shows a type I isotherm, characterized by an abrupt knee at the low relative pressure followed by a slight increase in the nitrogen uptake at the high relative pressure, indicating that micropores mainly constitute the porosity of these samples. The rapid growth towards a plateau at the low relative pressure suggests low or null mesoporosity. A BET surface area of 465 m<sup>2</sup>·g<sup>-1</sup> and a total pore volume of 0.182 cm<sup>3</sup>·g<sup>-1</sup> were estimated for the 3DeCMF structure. Figure S4 displays the CO<sub>2</sub> adsorption isotherm of the material obtained at 273 K. The sample shows a narrow distribution of micropores with an average diameter of 0.5 nm, larger than the size of lithium ions (0.115 nm).

The XRD pattern of the 3DeCMFs presents two weak and broad peaks at 23° and 43° corresponding to the (002) and (100) diffraction modes (Figure 2e), characteristic of the disordered carbon material [31]. In addition, the broad signal corresponds to large variations in

This is the author's peer reviewed, accepted manuscript. However, the online version of record will be different from this version once it has been copyedited and typeset.

PLEASE CITE THIS ARTICLE AS DOI: 10.1063/1.50151949

the layer spacing of this structure, indicative of mostly disordered carbon. The interlayer spacing ( $d_{002}$ ) is calculated to be 0.370 nm [32]. The ability for lithium-ion storage is qualitatively estimated through the simple empirical parameter  $R$  defined by Dahn et al. [22]. According to this,  $R$  decreases as the single-layer content of the carbon increases, showing a direct relationship with the ability for lithium-ion storage. A value of  $R = 2.3$  is obtained from the quotient between the height and the background of a 002 peak, which is illustrated in Figure 2g. This indicates a partial degree of graphitization, with a concentration of single layers in the carbon materials amounting to ~30 %, similar to other electrospun carbon nanofibers [18].

Raman spectroscopy was applied to yield detailed information on the degree of structural disorder of this material. The spectra from Figure 2f show two characteristically vibrational bands at 1350 and 1600  $\text{cm}^{-1}$ ; these bands are assigned to disordered carbon (D band) and graphitic carbon (G band), respectively [33]. Unlike graphite, where a sharp peak is observed at 1600  $\text{cm}^{-1}$ , both vibrational signals present a broad distribution, which requires a signal deconvolution procedure. This result confirms the presence of partially graphitized carbon, together with amorphous carbon. The intensity ratio of the deconvoluted D/G bands indicates the ratio of each carbon type, which in this material is found to be  $I_D/I_G = 2.62$  [34]. In fact, there is a tradeoff between pliability (less brittle) and electronic conductivity for electro spun carbon freestanding fibers. This is a well-established consideration in process of these fibers. Herein, we applied 850°C in line with similar works [35]. From all the above analyses, the porous 3DeCMFs display optimal microstructural characteristics to be used as anode materials in LIBs because the graphitic structure of the pore walls can favor lithium intercalation under an electrochemical stimulus whereas the relatively high specific surface area can help enhance the interfacial contact. As the electrospun fibers mainly present a partially graphitized disordered structure, ion storage behavior will likely be halfway between hard carbons and graphitic materials [36], which also indicative of their suitability not only for lithium-ion storage but also for other technologies such as Na-ion batteries.

This is the author's peer reviewed, accepted manuscript. However, the online version of record will be different from this version once it has been copyedited and typeset.

PLEASE CITE THIS ARTICLE AS DOI: 10.1063/1.50151949

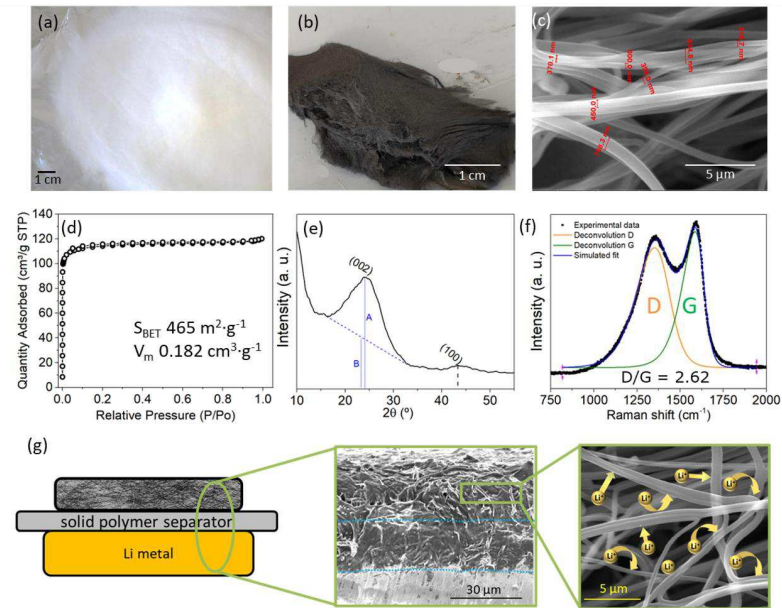


FIG2. Characterization of the 3D electrospun fibers through optical imaging (a) after electrospinning and (b) after carbonization. (c) Scanning electron microscopy image of the 3DeCMFs and the fiber thickness. (d) Adsorption isotherms with nitrogen (-196 °C), surface area, and specific volume calculations. Structural characterization of 3DeCMFs through (e) XRD and (f) Raman Spectroscopy. (g) Configuration of the cell for electrochemical measurements and SEM of the cell cross-section and the 3DeCMFs.

The electrochemical characterization of the 3DeCMFs was carried out in cells with the mentioned configuration having either liquid or solid electrolyte. For the former, the 3DeCMFs were assembled against a Li metal using a Celgard® separator [37]. Figure 2g shows the configuration with a Li metal electrode and an electrolyte separator used in this study. The cross-section of the cell clearly shows an intimate contact between the solid electrolyte in the 3DeCMF pores and the electrolyte/Li-metal interface, attributed to their wettability, which is crucial to the operation of SSBs.



This is the author's peer reviewed, accepted manuscript. However, the online version of record will be different from this version once it has been copyedited and typeset.

PLEASE CITE THIS ARTICLE AS DOI: 10.1063/1.50151949

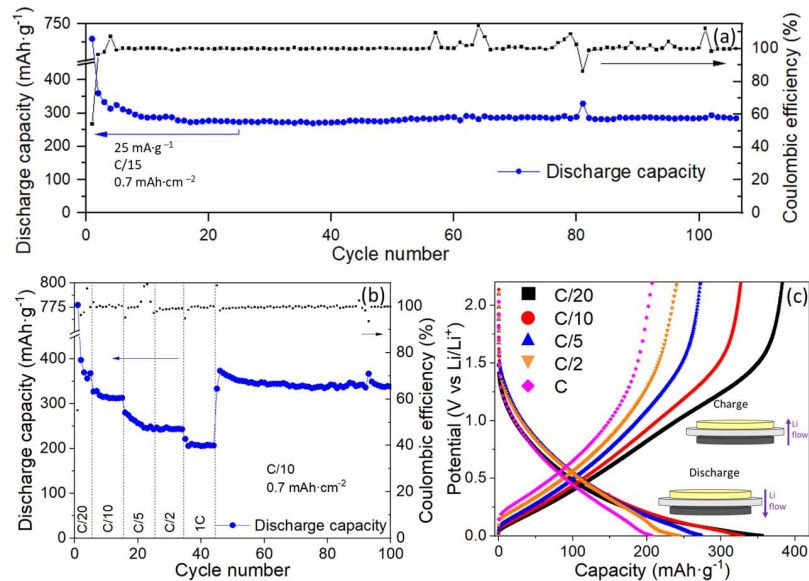


FIG3. Galvanostatic cycling of the electrospun carbon electrode against a Li metal electrode, using a 50:50 EC:PC 1M LiPF<sub>6</sub> electrolyte. (a) 100 charge-discharge cycles and coulombic efficiency at a constant current of 25 mA·g<sup>-1</sup> (C/15). (b) Rate capability test showing the charge-discharge capacity and coulombic efficiency as a function of the cycle number from C/20 to 1 C and back to C/10. (c) Voltage profiles at increasing C-rate from C/20 up to 1 C.

The low coulombic efficiency of ca. 50% observed during the first cycle of the cell at constant current, in Figure 3a, is ascribed to an irreversible capacity of 330 mAh g<sup>-1</sup> attained during the discharge step at a potential around 0.7 V vs. Li/Li<sup>+</sup> (Figure S5). Such irreversible capacity loss is ascribed to the electrolyte decomposition and solid electrolyte interphase (SEI) formation in line with the literature [38]. The excess Li consumption can also be explained by the reaction between the electrolyte and the carbon nanostructures due to the high surface area of the 3DeCMF materials (385 m<sup>2</sup>·g<sup>-1</sup>, Figure 2d), resulting in an appreciable voltage hysteresis during the charging process (Figure S5) [39]. After the initial cycles where the capacity faded quickly (first ten cycles), the 3DeCMF electrode stabilizes the discharge capacity delivering 350-300 mAh g<sup>-1</sup>

This is the author's peer reviewed, accepted manuscript. However, the online version of record will be different from this version once it has been copyedited and typeset.

PLEASE CITE THIS ARTICLE AS DOI: 10.1063/1.50151949

with ca. 99% coulombic efficiency. For the rest of the cycles, the capacity retention was above 80 %, with a similar coulombic efficiency. In addition, the lack of a low-voltage plateau indicates no filling of the closed porosity, suggesting the intercalation of lithium in the interlayer to be a single  $\text{Li}^+$  build-up mechanism for 3DeCMF electrodes.

The rate capability test shows discharge capacity values of  $360 \text{ mAh}\cdot\text{g}^{-1}$  at C/20 and remains as high as  $200 \text{ mAh}\cdot\text{g}^{-1}$  at 1 C (Figure 3b). The polarization of the cell during the charge and discharge step increases with the increasing current, likely due to kinetic limitations (Figure 3c). A higher polarization is observed during the charging step (assuming irregular Li-metal plating at higher currents) in comparison to the discharge, but this did not prevent the remarkable recovery of the cell at C/10, delivering  $350 \text{ mAh}\cdot\text{g}^{-1}$  (Figure 3b). The CE remained at 99% for most of the cycles. In addition, the  $\text{Li}^+$  intercalation profile displays similarities between ordered and disordered carbons, which show  $\text{Li}^+$  intercalation predominantly below 0.5 V [40], and homogeneously at different voltages with a smoother initial slope [41], respectively. This is the expected behavior for the mixed ordered-disordered nature of the fibers (Figure 2) and is similar to the  $\text{Li}^+$  intercalation profiles of electrospun materials in the literature [18].

Considering the above, we analyzed the electrochemical behavior of these electrodes in SSBs configuration (Figure 2g). The replacement of the liquid electrolyte with a solid counterpart is challenging mainly due to the larger solid-solid resistive interfaces and polarization, jeopardizing the performance of the cells. Here, the porous electrode of 3DeCMFs was filled with a slurry containing a PEO and LiBOB as a solid electrolyte; additionally, a self-standing membrane of PEO-LiBOB was used as an SPE separator to assemble half cells with a Li metal. The LiBOB salt was selected over fluorinated lithium salts to avoid fluor-based decomposition products produced at low redox potentials [42–44]. The cells were conditioned at 70 °C for 24 hours to minimize interfacial resistance by softening the polymer. Figure S6 shows the SEM image of a cross-section of the cell after conditioning, evidencing the complete wetting of fibers, which leads to excellent interlayer adhesion between the 3DeCMF electrode and the SPE separator (an

This is the author's peer reviewed, accepted manuscript. However, the online version of record will be different from this version once it has been copyedited and typeset.

PLEASE CITE THIS ARTICLE AS DOI: 10.1063/5.0151949

intimate contact was also observed between the SPE and the Li metal electrode). Figure 4 gathers the galvanostatic cycling of the solid-state cells.

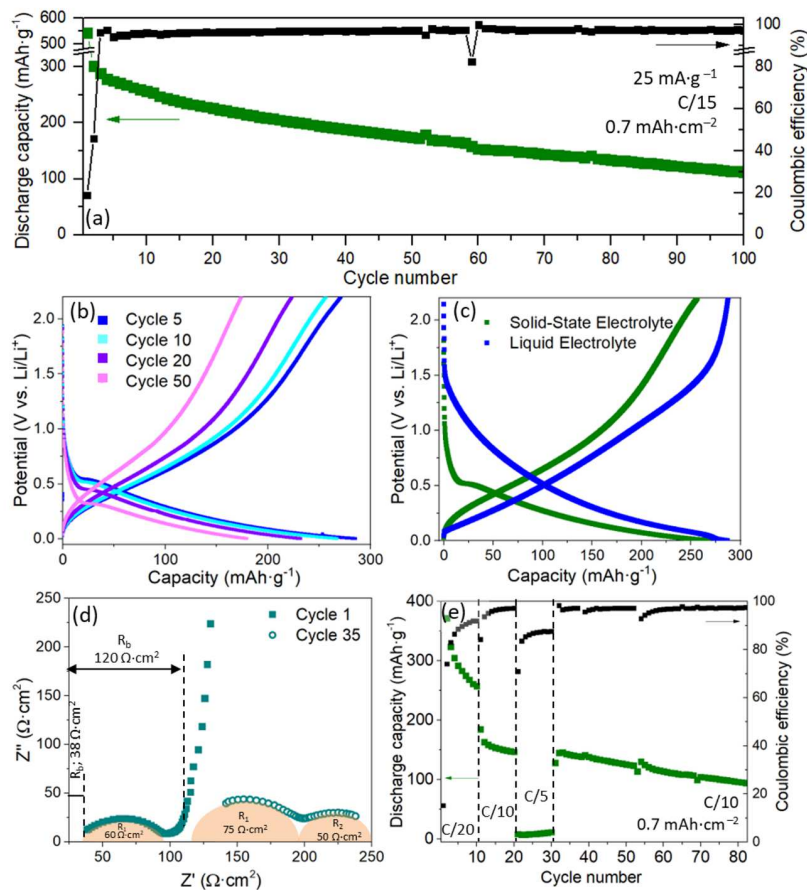


FIG4. Galvanostatic cycling of the electrospun carbon electrode (3DeCMF) against a Li metal electrode, using a PEO–LiBOB (EO:Li 20:1) SPE separator. (a) Discharge capacity as a function of the cycle number under a constant current of  $25 \text{ mA}\cdot\text{g}^{-1}$  (C/15). (b) Voltage profiles at different cycles ( $25 \text{ mA}\cdot\text{g}^{-1}$ , C/15), (c) Voltage profiles of the 10<sup>th</sup> cycle for PEO–LiBOB solid electrolyte

This is the author's peer reviewed, accepted manuscript. However, the online version of record will be different from this version once it has been copyedited and typeset.

PLEASE CITE THIS ARTICLE AS DOI: 10.1063/1.50151949

and EC:PC-LiPF<sub>6</sub> liquid electrolyte at 25 mA·g<sup>-1</sup>. (d) EIS profile of the PEO-LiBOB solid electrolyte cell before cycling and after 35 cycles. (e) Discharge capacity as a function of the C-rate.

Figure 4a shows a larger irreversible capacity during the initial cycles of the cell, yielding a much lower coulombic efficiency (18%) compared to the liquid-electrolyte cell (50%). This is in agreement with previous literature, where the SEI formation and likely reduction of Li salt restrict this performance (Figure 4a) [16,45,46]. The CE increases up to 97% just after the second cycle, and the discharge profiles display a small flat plateau of 20 mAh·g<sup>-1</sup> at ca. 0.5 V vs. Li/Li<sup>+</sup> followed by a sloping plateau (Figure 4b). The results shown in Figure S7 evidence a Li storage below 0.75 V and 0.02 V (vs Li/Li<sup>+</sup>), which is in line with the galvanostatic cycling results in Figure 4b-c. In terms of electrochemical stability from the CV, there are only small variations between cycle 2 and cycle 10, suggesting that the Li storage potential does not vary over cycling, even if a possible side reaction leads to a capacity fading (Figure 4a). Interestingly, the comparison of charge-discharge profiles between liquid and solid electrolyte cells demonstrates a difference in the lithium intercalation process (Figure 4c) in terms of the lithiation potential (vs Li/Li<sup>+</sup>): the intercalation begins at 1.5 V for 3DeCMFs with liquid electrolytes while it occurs below 0.5 V in the case of SSBs. The onset of the lithium transfer process from the SPE to the 3DeCMFs is delayed compared to the liquid electrolyte, as evidenced by a larger overpotential. Also, it cannot be ruled out that the SEI layer formed by the reduction products of the anion (BOB<sup>-</sup>) and concentrated in the graphitized carbon regions, leading to the variation of Li<sup>+</sup> intercalation.

The average discharge capacity during the initial cycles is 300 mAh·g<sup>-1</sup> at C/20, with a stable coulombic efficiency above 96 %. However, the capacity decreases down to 200 mAh·g<sup>-1</sup> after 35 cycles, and 110 mAh·g<sup>-1</sup> in the 100<sup>th</sup> cycle, suggesting continuous parasitic reactions across these electrodes, which needs further optimization efforts. The EIS in Figure 4d shows an increase in the bulk cell resistance (38 to 120 Ω·cm<sup>2</sup>), maintaining the initial interfacial resistance ascribed to the electrode/electrolyte interface (R<sub>1</sub>, C = 10<sup>-6</sup> F). The presence of an additional high-capacitance semicircle in the cell (R<sub>2</sub>, C = 10<sup>-4</sup> F), is likely ascribed to such side-reaction

This is the author's peer reviewed, accepted manuscript. However, the online version of record will be different from this version once it has been copyedited and typeset.

PLEASE CITE THIS ARTICLE AS DOI: 10.1063/1.50151949

occurring in the 3DeCMF during cycling. The reaction products may lead to an overall increase in cell resistance and a decrease in the active sites available for ion intercalation, which can potentially explain why the capacity faded gradually. The rate performance in Figure 4e shows that the solid electrolyte cell suffers from kinetic limitations ascribed to low ionic conductivity compared to the liquid electrolyte, as can be clearly seen from the cell response at higher rates. Discharge capacity values at C/20 and C/10 remain between 250 and 150 mAh·g<sup>-1</sup>, respectively. At higher current values, the capacity decreases dramatically, which is indicative of such kinetic limitations; however, the cell was still able to recover at C/10 for another 50 cycles, with a discharge capacity around 100 mAh·g<sup>-1</sup> and a coulombic efficiency of 97%.

The integration of carbonized fiber electrodes into solid-state batteries takes advantage of their wetting properties and intimate interfacial connection. Despite a significant irreversible capacity, the solid electrolyte cells with fiber electrodes delivered a discharge capacity of over 150 mAh·g<sup>-1</sup> with 100% coulombic efficiency. However, the observed gradual capacity fade was attributed to parasitic reactions increasing the cell resistance and the blockage of active sites for ion storage. The Li<sup>+</sup> intercalation into these fibers was found to be occurring at more negative potentials compared to liquid cells and to be intermediate between graphite and hard carbon. In the present work, the application of carbon microfibers in solid-state batteries and performance assessment represents progress towards viable carbon fibre-based solid-state anode. The recent and single report on the use of carbon fibres as an anode in SSBs reports specific capacities up to 92 mAh/g [8]. Our solid-state cells delivered a higher capacity, up to 300 mAh/g, highlighting the remarkable progress in performance, arising from the careful materials design and efforts to decrease interfacial resistance of the solid-state cell. These results open a wide range of opportunities, where the use and optimization of free-standing carbon fiber electrodes as anodes can endow all-solid-state batteries with high energy density and safety. The use of carbon fiber anodes can also be potentially extended to other battery chemistries and electrochemical devices where highly networked and seamless interfacial connections can offer advantages.

This is the author's peer reviewed, accepted manuscript. However, the online version of record will be different from this version once it has been copyedited and typeset.

PLEASE CITE THIS ARTICLE AS DOI: 10.1063/1.50151949

### Supplementary Material

See the supplementary material for the details of electrospinning mesh fabrication, electrolyte preparation, 3D electrospun fiber characterization, electrochemical characterization, and sheet resistance and tensile test measurements.

### Acknowledgments

The authors would like to acknowledge the support given by Dr. Enterria with the physical characterization of the electrodes. Dr. Saurel is acknowledged for the enriching comments and discussion regarding the electrochemical application of the materials. Ministerio de Ciencia, Innovación y Universidades of Spain is greatly acknowledged for the Juan de la Cierva grant under the reference IJCI-2017-32310. CG acknowledges the Royal Society, London for a URF (Grant no. UF160573).

### AUTHOR DECLARATIONS

#### Conflict of interests

The authors declare no conflict of competing interests.

#### Author contributions

**Mikel Arrese-Igor:** investigation, validation, visualization, writing; **Michel Vong:** investigation; **Ander Orue:** investigation, visualization; **Panagiotis Kassanos:** investigation; **Chandramohan George:** investigation, writing, reviewing; **Frédéric Aguesse:** conceptualization, funding acquisition; **Roman Mysyk:** writing, reviewing; **Norbert Radacsi:** writing, reviewing; **Pedro López-Aranguren:** conceptualization, writing, supervision, reviewing.

#### Data Availability

The data that support the findings of this study are available within the article.

### References

This is the author's peer reviewed, accepted manuscript. However, the online version of record will be different from this version once it has been copyedited and typeset.

PLEASE CITE THIS ARTICLE AS DOI: 10.1063/1.50151949

1. Budde-Meiwes H, Drillkens J, Lunz B, Muennix J, Rothgang S, Kowal J, et al. A review of current automotive battery technology and future prospects. Proceedings of the Institution of Mechanical Engineers, Part D: Journal of Automobile Engineering. 2013 Apr 19;227(5):761–76.
2. Palacín MR. Recent advances in rechargeable battery materials: a chemist's perspective. Chem Soc Rev. 2009;38(9):2565–75.
3. Owen JR. Rechargeable lithium batteries. Chem Soc Rev. 1997;26(4):259–67.
4. Goodenough JB, Kim Y. Challenges for Rechargeable Li Batteries. Chem Mater. 2010 Feb 9;22(3):587–603.
5. Tarascon JM, Armand M. Issues and challenges facing rechargeable lithium batteries. Nature. 2001 Nov 1;414(6861):359–67.
6. Armand M, Tarascon JM. Building better batteries. Nature. 2008 Feb 6;451:652.
7. Ohsaki T, Kishi T, Kuboki T, Takami N, Shimura N, Sato Y, et al. Overcharge reaction of lithium-ion batteries. Journal of Power Sources. 2005 Aug 26;146(1):97–100.
8. Eshetu GG, Judez X, Li C, Martinez-Ibañez M, Sanchez-Diez E, Rodriguez-Martinez LM, et al. Solid Electrolytes for Lithium Metal and Future Lithium-ion Batteries. In: Future Lithium-ion Batteries. Royal Society of Chemistry; 2019. p. 72–101.
9. Nam YJ, Oh DY, Jung SH, Jung YS. Toward practical all-solid-state lithium-ion batteries with high energy density and safety: Comparative study for electrodes fabricated by dry- and slurry-mixing processes. J Power Sources. 2018 Jan 31;375:93–101.
10. Janek J, Zeier WG. A solid future for battery development. Nature Energy. 2016 Sep 8;1:16141.
11. Wang S, Fang R, Li Y, Liu Y, Xin C, Richter FH, et al. Interfacial challenges for all-solid-state batteries based on sulfide solid electrolytes. Journal of Materiomics [Internet]. 2020 Sep 10; Available from: <http://www.sciencedirect.com/science/article/pii/S2352847820303713>
12. Golozar M, Paolella A, Demers H, Savoie S, Girard G, Delaporte N, et al. Direct observation of lithium metal dendrites with ceramic solid electrolyte. Sci Rep. 2020 Oct 27;10(1):18410.
13. Commarieu B, Paolella A, Collin-Martin S, Gagnon C, Vijn A, Guerfi A, et al. Solid-to-liquid transition of polycarbonate solid electrolytes in Li-metal batteries. J Power Sources. 2019 Oct;436:226852.
14. Sun YK. Promising All-Solid-State Batteries for Future Electric Vehicles. ACS Energy Lett. 2020 Oct 9;5(10):3221–3.
15. Varzi A, Raccichini R, Passerini S, Scrosati B. Challenges and prospects of the role of solid electrolytes in the revitalization of lithium metal batteries. J Mater Chem A. 2016;4(44):17251–9.

This is the author's peer reviewed, accepted manuscript. However, the online version of record will be different from this version once it has been copyedited and typeset.

PLEASE CITE THIS ARTICLE AS DOI: 10.1063/5.0151949

16. Homann G, Stolz L, Nair J, Laskovic IC, Winter M, Kasnatscheew J. Poly(Ethylene Oxide)-based Electrolyte for Solid-State-Lithium-Batteries with High Voltage Positive Electrodes: Evaluating the Role of Electrolyte Oxidation in Rapid Cell Failure. *Sci Rep.* 2020 Mar 9;10(1):4390.
17. Goutam S, Omar N, Bossche PVD, Mierlo JV. Chapter Two - Review of Nanotechnology for Anode Materials in Batteries. In: Rodriguez-Martinez LM, Omar N, editors. *Emerging Nanotechnologies in Rechargeable Energy Storage Systems* [Internet]. Boston: Elsevier; 2017. p. 45–82. (Micro and Nano Technologies). Available from: <http://www.sciencedirect.com/science/article/pii/B9780323429771000029>
18. Kumar PS, Sahay R, Aravindan V, Sundaramurthy J, Ling WC, Thavasi V, et al. Free-standing electrospun carbon nanofibres—a high performance anode material for lithium-ion batteries. *Journal of Physics D: Applied Physics.* 2012 Jun;45(26):265302.
19. Li G, Liu Z, Huang Q, Gao Y, Regula M, Wang D, et al. Stable metal battery anodes enabled by polyethylenimine sponge hosts by way of electrokinetic effects. *Nature Energy.* 2018 Dec 1;3(12):1076–83.
20. Liu N, Lu Z, Zhao J, McDowell MT, Lee HW, Zhao W, et al. A pomegranate-inspired nanoscale design for large-volume-change lithium battery anodes. *Nature Nanotechnology.* 2014 Mar 1;9(3):187–92.
21. Wang HG, Yuan S, Ma DL, Zhang XB, Yan JM. Electrospun materials for lithium and sodium rechargeable batteries: from structure evolution to electrochemical performance. *Energy Environ Sci.* 2015;8(6):1660–81.
22. Liu Y, Xue JS, Zheng T, Dahn JR. Mechanism of lithium insertion in hard carbons prepared by pyrolysis of epoxy resins. *Carbon.* 1996 Jan 1;34(2):193–200.
23. Morris RS, Dixon BG, Gennett T, Raffaella R, Heben MJ. High-energy, rechargeable Li-ion battery based on carbon nanotube technology. *J Power Sources.* 2004 Nov 15;138(1):277–80.
24. Kim C, Yang KS, Kojima M, Yoshida K, Kim YJ, Kim YA, et al. Fabrication of Electrospinning-Derived Carbon Nanofiber Webs for the Anode Material of Lithium-Ion Secondary Batteries. *Advanced Functional Materials.* 2006;16(18):2393–7.
25. Ko F, Gogotsi Y, Ali A, Naguib N, Ye H, Yang GL, et al. Electrospinning of Continuous Carbon Nanotube-Filled Nanofiber Yarns. *Advanced Materials.* 2003 Jul 17;15(14):1161–5.
26. Kim C, Yang KS. Electrochemical properties of carbon nanofiber web as an electrode for supercapacitor prepared by electrospinning. *Appl Phys Lett.* 2003 Aug 5;83(6):1216–8.
27. Vong M, Speirs E, Klomkliang C, Akinwumi I, Nuansing W, Radacsi N. Controlled three-dimensional polystyrene micro- and nano-structures fabricated by three-dimensional electrospinning. *RSC Advances.* 2018;8(28):15501–12.
28. Vong M, Diaz Sanchez FJ, Keirouz A, Nuansing W, Radacsi N. Ultrafast fabrication of Nanofiber-based 3D Macrostructures by 3D electrospinning. *Materials & Design.* 2021 Oct 1;208:109916.



This is the author's peer reviewed, accepted manuscript. However, the online version of record will be different from this version once it has been copyedited and typeset.

PLEASE CITE THIS ARTICLE AS DOI: 10.1063/1.50151949

29. Wu F, Zhang K, Liu Y, Gao H, Bai Y, Wang X, et al. Polymer electrolytes and interfaces toward solid-state batteries: Recent advances and prospects. *Energy Storage Materials*. 2020 Dec 1;33:26–54.
30. Ogawa H, Saito K. Oxidation behavior of polyacrylonitrile fibers evaluated by new stabilization index. *Carbon*. 1995 Jan 1;33(6):783–8.
31. Chen T, Liu Y, Pan L, Lu T, Yao Y, Sun Z, et al. Electrospun carbon nanofibers as anode materials for sodium ion batteries with excellent cycle performance. *J Mater Chem A*. 2014;2(12):4117–21.
32. Xu B, Wu MS, Liu G, Ouyang CY. Understanding the effect of the layer-to-layer distance on Li-intercalated graphite. *Journal of Applied Physics*. 2012 Jun 15;111(12):124325.
33. Ferrari AC, Robertson J. Interpretation of Raman spectra of disordered and amorphous carbon. *Phys Rev B*. 200AD;61(20):14095–107.
34. Ammar MR, Rouzaud JN. How to obtain a reliable structural characterization of polished graphitized carbons by Raman microspectroscopy. *Journal of Raman Spectroscopy*. 2012;43(2):207–11.
35. Liu X, Ouyang M, Orzech MW, Niu Y, Tang W, Chen J, et al. In-situ fabrication of carbon-metal fabrics as freestanding electrodes for high-performance flexible energy storage devices. *Energy Storage Materials*. 2020 Sep 1;30:329–36.
36. Dou X, Hasa I, Saurel D, Vaalma C, Wu L, Buchholz D, et al. Hard carbons for sodium-ion batteries: Structure, analysis, sustainability, and electrochemistry. *Materials Today*. 2019;23:87–104.
37. Xu K. Nonaqueous Liquid Electrolytes for Lithium-Based Rechargeable Batteries. *Chem Rev*. 2004 Oct 1;104(10):4303–418.
38. Endo M, Kim C, Nishimura K, Fujino T, Miyashita K. Recent development of carbon materials for Li ion batteries. *Carbon*. 2000 Jan 1;38(2):183–97.
39. Subramanian V, Zhu H, Wei B. High Rate Reversibility Anode Materials of Lithium Batteries from Vapor-Grown Carbon Nanofibers. *J Phys Chem B*. 2006 Apr 1;110(14):7178–83.
40. Winter M, Besenhard JO, Spahr ME, Novák P. Insertion Electrode Materials for Rechargeable Lithium Batteries. *Advanced Materials*. 1998 Jul 1;10(10):725–63.
41. Chen Y, Li X, Zhou X, Yao H, Huang H, Mai YW, et al. Hollow-tunneled graphitic carbon nanofibers through Ni-diffusion-induced graphitization as high-performance anode materials. *Energy Environ Sci*. 2014;7(8):2689–96.
42. Xiang H, Shi P, Bhattacharya P, Chen X, Mei D, Bowden ME, et al. Enhanced charging capability of lithium metal batteries based on lithium bis(trifluoromethanesulfonyl)imide-lithium bis(oxalato)borate dual-salt electrolytes. *J Power Sources*. 2016 Jun 30;318:170–7.

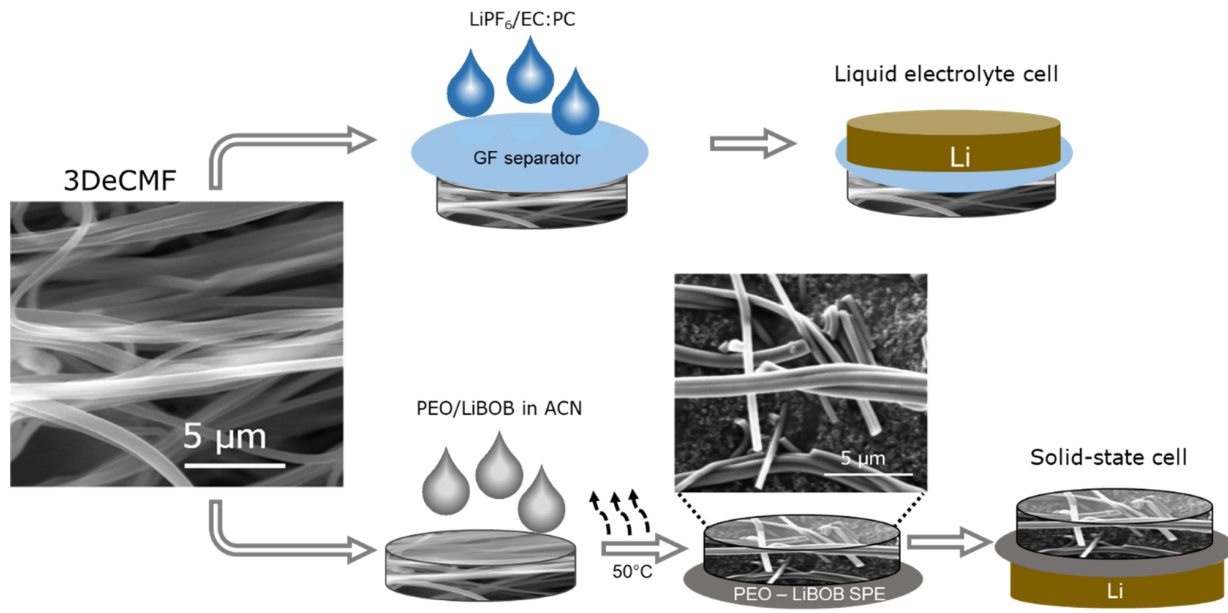
This is the author's peer reviewed, accepted manuscript. However, the online version of record will be different from this version once it has been copyedited and typeset.

PLEASE CITE THIS ARTICLE AS DOI: 10.1063/1.50151949

43. Ismail I, Noda A, Nishimoto A, Watanabe M. XPS study of lithium surface after contact with lithium-salt doped polymer electrolytes. *Electrochim Acta*. 2001 Mar 15;46(10):1595–603.
44. Judez X, Zhang H, Li C, González-Marcos JA, Zhou Z, Armand M, et al. Lithium Bis(fluorosulfonyl)imide/Poly(ethylene oxide) Polymer Electrolyte for All Solid-State Li-S Cell. *J Phys Chem Lett*. 2017 May 4;8(9):1956–60.
45. Xu K, Lee U, Zhang S, Wood M, Jow RT. Chemical Analysis of Graphite/Electrolyte Interface Formed in LiBOB-Based Electrolytes. *Electrochem Solid-State Lett*. 2003;6(7).
46. Parimalam BS, Lucht BL. Reduction Reactions of Electrolyte Salts for Lithium Ion Batteries: LiPF<sub>6</sub>, LiBF<sub>4</sub>, LiDFOB, LiBOB, and LiTFSI. *J Electrochem Soc*. 2018;165(2).

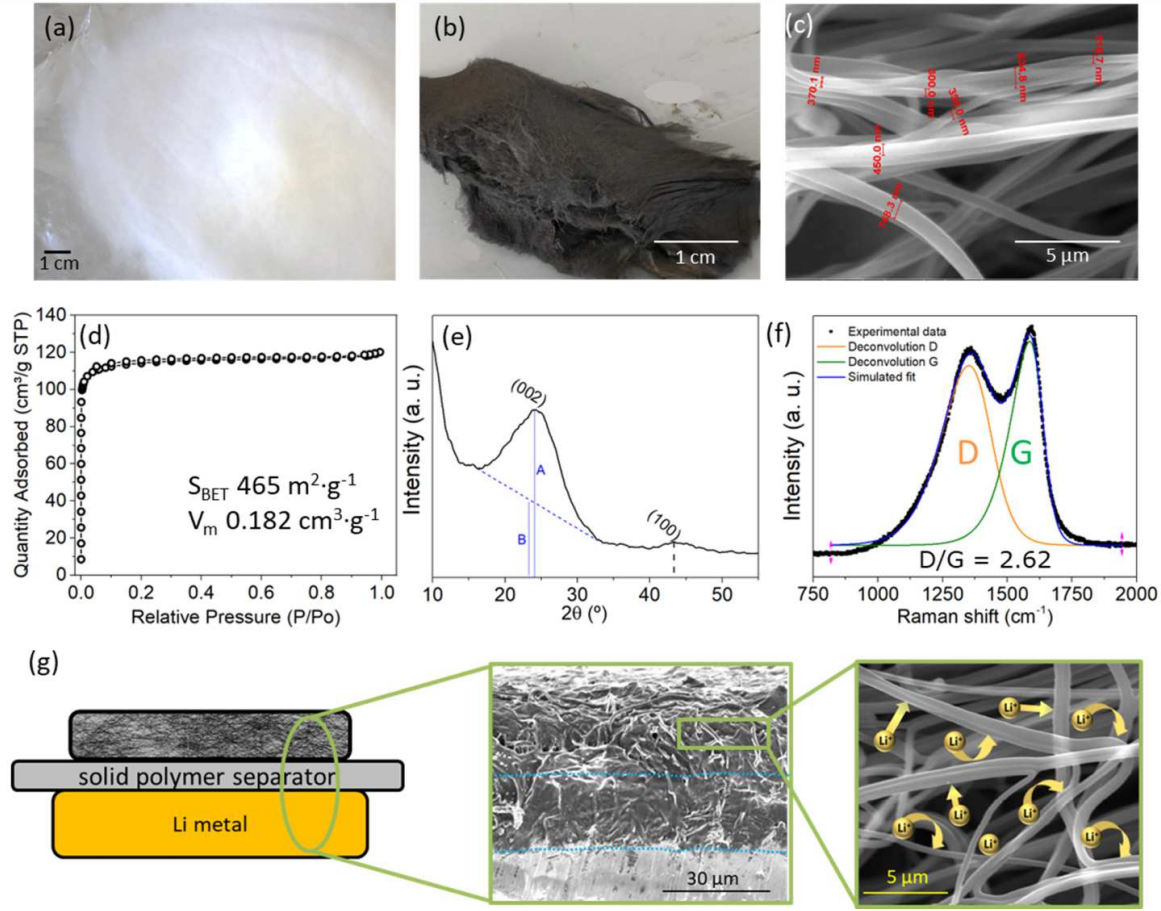
This is the author's peer reviewed, accepted manuscript. However, the online version of record will be different from this version once it has been copyedited and typeset.

PLEASE CITE THIS ARTICLE AS DOI: 10.1063/1.50151949



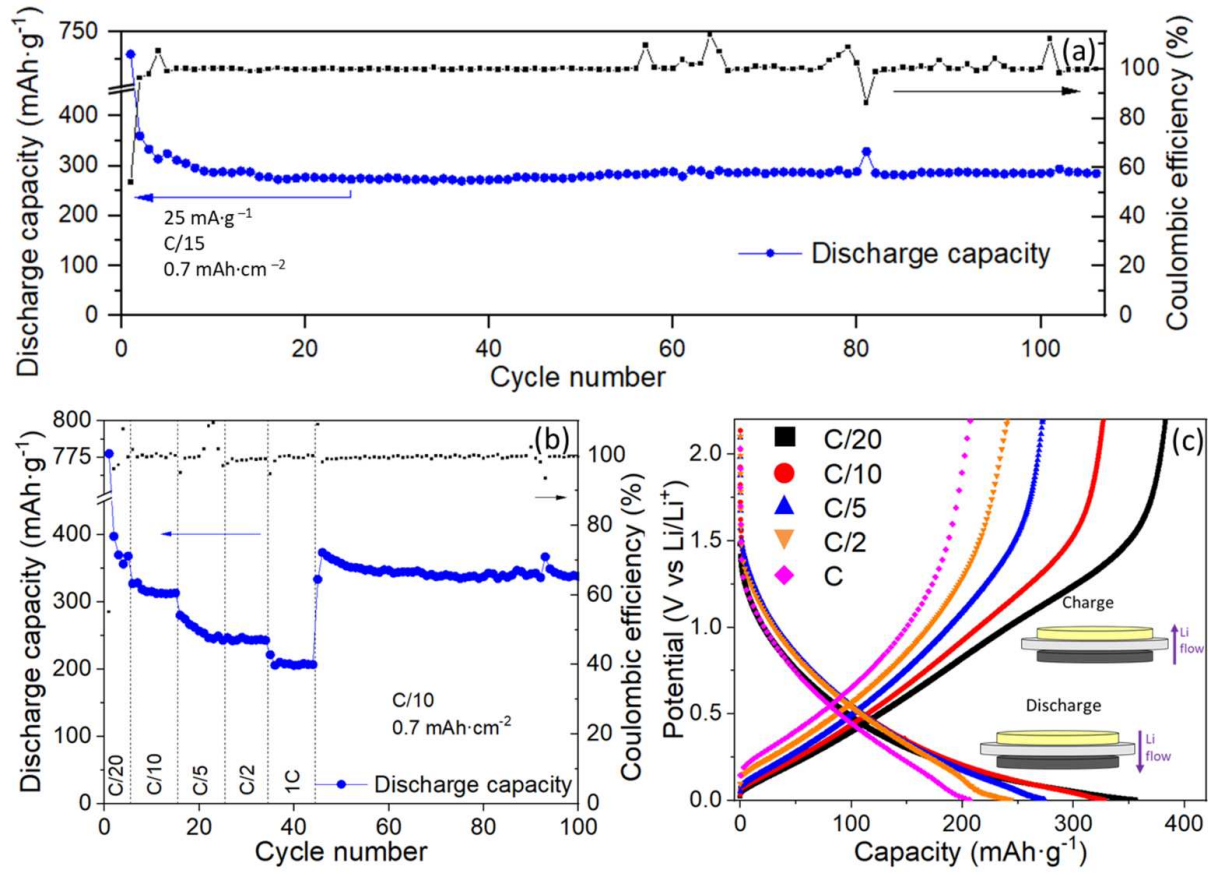
This is the author's peer reviewed, accepted manuscript. However, the online version of record will be different from this version once it has been copyedited and typeset.

PLEASE CITE THIS ARTICLE AS DOI: 10.1063/5.0151949



This is the author's peer reviewed, accepted manuscript. However, the online version of record will be different from this version once it has been copyedited and typeset.

PLEASE CITE THIS ARTICLE AS DOI: 10.1063/1.50151949



This is the author's peer reviewed, accepted manuscript. However, the online version of record will be different from this version once it has been copyedited and typeset.

PLEASE CITE THIS ARTICLE AS DOI: 10.1063/5.0151949

